



Cite this: DOI: 10.1039/c7nj01553d

Received 8th May 2017,  
Accepted 22nd June 2017

DOI: 10.1039/c7nj01553d

rsc.li/njc

# Temperature-dependent water penetration in Tween20:cholesterol niosome membrane: a study using excited state prototropism of 1-naphthol†

Jitendriya Swain, Jhili Mishra, Akanksha Singh and Ashok Kumar Mishra \*

This work uses the dynamics of the excited state proton transfer of 1-naphthol to water as a basis for understanding the temperature-dependent changes in the water accessibility of the niosome membrane domain. The decrease in the neutral form fluorescence intensity of membrane bound 1-naphthol, the significant drop in the membrane-bound anion form fluorescence lifetime, and the changes in the fluorescence lifetime distribution plots of the two prototropic forms of 1-naphthol indicate a regular increase in the water penetration in the interfacial region of the niosome membrane domain, whereas the dry core regions appear unaffected with increasing temperature (10–60 °C). Unlike some liposomes and niosomes, these niosomes do not show thermotropic phase transition behavior.

## Introduction

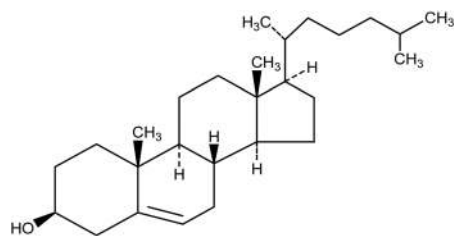
The structural arrangements and confined microenvironments of organized systems play an important role in many biological and photophysical processes.<sup>1,2</sup> Excited state proton transfer processes are known to be markedly affected by the confined microenvironments of cyclodextrins, lipid bilayer membranes, proteins, polymers, micelles, micro-emulsions, *etc.*<sup>1</sup> It is well known that many aromatic amines and phenols are more acidic in the excited state, and these molecules are called photoacids.<sup>3</sup> Among the aromatic phenols, 1-naphthol (1-NpOH) is a well-known photoacid ( $pK_a = 9.2$ ,  $pK_a^* = 0.4$ ) in the excited singlet state.<sup>4</sup> In aqueous medium, the excited state deprotonation rate of 1-NpOH is  $2.5 \times 10^{10} \text{ s}^{-1}$ .<sup>4</sup> It has been shown that in aqueous medium  $4 \pm 1$  water molecules associate to form a cluster which acts as a base.<sup>5,6</sup> As a result of this fast deprotonation, the intensity of the neutral emission (370 nm) of 1-NpOH is extremely low and only anion emission (470 nm) is observed. The excited state proton transfer of 1-NpOH is significantly retarded in nonaqueous media like alcohols or in the hydrophobic domains of organized systems and a predominant neutral form emission is observed.<sup>7–9</sup> Although the excited state proton transfer (ESPT) process of 1-NpOH is well known in cyclodextrin,<sup>10</sup> lipid bilayer membranes,<sup>11</sup> polymers<sup>7</sup> and different solvent mixtures,<sup>12</sup> there has been no report available on the ESPT process of 1-NpOH in niosome membranes.

1-Naphthol is a very good ESPT fluorescent molecular probe because of its environment-dependent emission bands, distributive nature, small size, and low perturbation imparted to the system.<sup>13</sup> Along with all these properties, the fluorescence lifetime and the corresponding amplitude of the different prototropic emissions of 1-NpOH are sensitive indicators for the level of hydration across the liposome membrane, as explained by Monalisa *et al.*<sup>14</sup> In this context we have tried to monitor the temperature-dependent changes in the level of hydration in niosome membranes using 1-NpOH as a fluorescent molecular probe. Structurally, niosomes are similar to liposomes having a vesicular structure with a lumen containing water and a membrane.<sup>15,16</sup> The membrane regions of niosomes and liposomes are broadly subdivided into two domains: the water facing interfacial domain, which is often strongly hydrated, and the membrane core domain, which is water deficient in nature.<sup>15–18</sup> However, the constituent molecules of the two systems are different, and therefore the niosome membranes are different in some ways: (i) niosome membranes are thicker than lipid bilayer membranes<sup>19</sup> and (ii) the cores of the niosomal membranes are not as dry as the cores of the lipid bilayer membranes.<sup>20</sup> Both liposomes and niosomes are well-known drug carriers. Niosomes offer some advantages over liposomes such as: (i) higher chemical stability and long storage time; (ii) relatively low cost of nonionic surfactants; (iii) high bio-compatibility and low toxicity;<sup>20</sup> and (iv) diversity of the constituent materials of niosomes enabling the possibility of significant cost reduction in preparing vesicular structures.

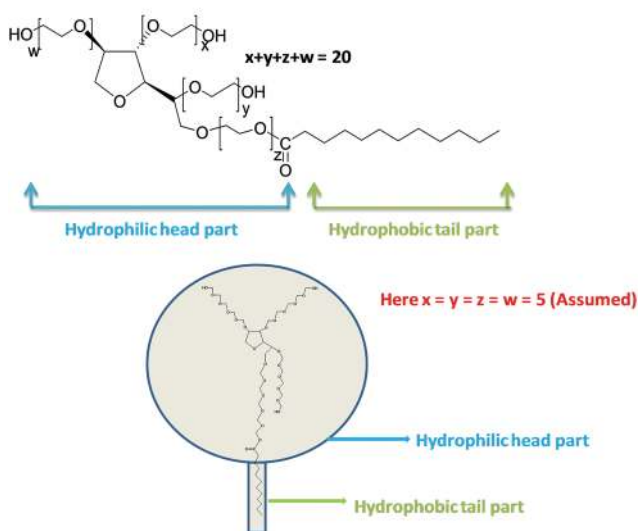
The niosomes prepared in the present study were composed of cholesterol and Tween20 (Scheme 1). Tween20 was chosen as a constituent for niosome preparation because of its low cost, bio-compatibility, and low toxicity.<sup>20</sup> It has a big hydrophilic

Department of Chemistry, Indian Institute of Technology Madras, Chennai 600 036, India. E-mail: mishra@iitm.ac.in

† Electronic supplementary information (ESI) available. See DOI: 10.1039/c7nj01553d



Cholesterol

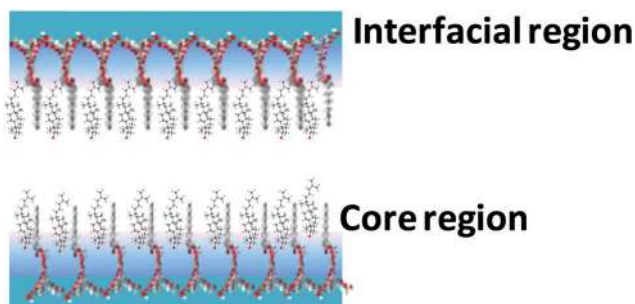


Tween20

Scheme 1 Chemical structure of cholesterol and Tween20.

head group and a short hydrophobic tail part (Scheme 1). With a very short tail as compared to the size of the head group, there is a necessity for cholesterol to form a stable bilayer membrane.<sup>17</sup> Scheme 2 represents the schematic diagram of niosome made up of cholesterol and TW20.

The study of the excited state proton transfer process of fluorescent molecules in the niosome microenvironment is rather scant. Bhattacharyya *et al.* showed the proton transfer process of pyranine in TX-100:cholesterol niosomes (size of the niosomes: 1000 nm).<sup>21</sup> Sarkar *et al.* studied the proton transfer process of 1'-hydroxy-2'-acetonaphthone (HAN), in Tween80:PEG-6000 niosome



Scheme 2 Schematic representation of the niosome bilayer membrane.

(size 0.2  $\mu\text{M}$ ) and the proton transfer process of curcumin in Tween20:cholesterol niosome (size 100 nm).<sup>17,22</sup> All these results explain the retardation of the excited state inter or intra molecular proton transfer (ESPT) process in niosome medium.

1-NpOH fluorescence is remarkably sensitive towards sol-gel phase transition induced changes in the level of hydration of lipid bilayer membranes.<sup>23</sup> This prompted us to use 1-NpOH as a fluorescent molecular probe to follow the temperature-induced changes in the level of water availability in the Tween20:cholesterol niosome membrane domain. This is the objective of the present work.

## Materials and methods

### Materials

1-Naphthol (1-NpOH) purchased from SRL, India, was sublimed and used after checking its purity. Tween20 (TW20) and cholesterol were purchased from Merck chemicals. The number 20 indicates the presence of 20 repeat units of polyethylene glycol in TW20 molecules. During the ethoxylation process these 20 monomeric units are distributed over four branches with varying values of  $x$ ,  $y$ ,  $z$  and  $w$ , keeping the total constant. Therefore, a common practice to represent the Tween20 group of molecules is  $x + y + z + w = 20$ .<sup>36</sup> All the solvents used were of spectroscopic grade. Triple-distilled water, prepared using alkaline permanganate, was used for the experiments.

### Methods

Dynamic light scattering (DLS) analysis was carried out using a Malvern Zetasizer nano series with a path length of 1 cm. The wavelength of the laser used was 632.8 nm and the scattering angle was kept as  $90^\circ$ . A transmission electron microscopy (TEM) image was taken by dropping a niosomal dispersion onto a carbon-coated copper grid in a Philips CM12 120 kV instrument. The copper grid was allowed to dry before the images were captured. Fluorescence emission measurements were performed using a Fluoromax-4 fluorescence spectrophotometer. Fluorescence lifetime measurements were carried out using a Horiba Jobin Yvon TCSPC lifetime instrument. A 295 nm nano-LED was used as the light source for the experiments. The pulse repetition rate was set to 1 MHz. The detector response time was less than 1 ns. The instrument response function (Prompt) was collected using a scatterer (Ludox AS40 colloidal silica). The decay data were analyzed using IBH software. A value of  $\chi^2$  in-between 0.99–1.3 with a symmetrical distribution of residuals was considered a good fit. The average lifetime values ( $\tau_{\text{avg}}$ ) were calculated using the following equation.<sup>14</sup>

$$\tau_{\text{avg}} = \left( \sum_{i=1}^n \alpha_i \tau_i^2 \right) / \left( \sum_{i=1}^n \alpha_i \tau_i \right)$$

IBH software was also used for lifetime distribution fitting having a  $\chi^2$  value between 0.99 and 1.3 using eqn (1), which was extracted from the DAS 6 manual.

$$F(t) = A + \sum_{k=1}^5 B_k [1 - (1 - q_k)t/\tau_k]^{1/1-q_k} \quad (1)$$

where  $\tau_k$  is the mean value of the lifetime distribution and  $q$  is a parameter of heterogeneity defined by

$$q = 1 + \frac{2}{N} = 1 + \frac{\langle(\gamma - \langle\gamma\rangle)^2\rangle}{\langle\gamma\rangle^2}$$

Here,  $q$  describes the fluctuation according to the mean value of the decay rate  $\langle\gamma\rangle = \langle\frac{1}{\tau}\rangle$ , which is also indicative of the width of the distribution and the number of decay channels ( $N$ ). The components of  $F(t)$  become exponentials as  $q_k$  tends towards one.

$$\left[1 - (1 - q_k)\frac{t}{\tau_k}\right]^{1/(1-q_k)} \xrightarrow{q_k \rightarrow 1} e^{-\frac{t}{\tau_k}}$$

The analysis software places limits on the value of  $q$  ( $1.01 \leq q \leq 1.3$ ), the lower limit representing  $q \rightarrow 1$ , and the upper limit allows the mean value of  $F(t)$  to be well defined. When  $q = 1.01$ , the lifetime tends towards a simple exponential term. When  $q = 1.3$ , the distribution of lifetimes is significantly larger.

### Niosome preparation

Standard methods for the preparation and characterization of niosomes from nonionic surfactants have been extensively reported in the literature.<sup>18,21,22,24,25</sup> Small unilamellar vesicles (SUVs) of TW20:cholesterol (1:1) were prepared using the solvent evaporation method as reported in the literature.<sup>18,24,25</sup> TW20:cholesterol (1:1) was dissolved in chloroform-methanol 2:1 (v/v). The concentrations of TW20 and cholesterol were kept at 1.25 mM, which is above the critical micellar concentration (CMC) of TW20 surfactant. The solution was evaporated to dryness. The solvent was removed using a rotary evaporator and residual solvent if any was removed by leaving the round bottom flask under vacuum for one hour. The niosome solution was prepared by adding the appropriate volume of phosphate buffer with a pH of 6.8 to the lipid film with vigorous vortexing at above 60 °C. The dispersion was then sonicated for 10 min at 60 °C using a probe-sonicator. Finally, the solution was centrifuged to remove free surfactants and larger vesicles. All the experiments were performed with a freshly prepared solution of niosome and fluorescent probes.

### Estimation of encapsulation efficiency of niosomes by 5-carboxyfluorescein release study

A niosome suspension was prepared in a  $10^{-5}$  M aqueous solution of 5-carboxyfluorescein (5-CF). The suspension was ultra-centrifuged at  $200\,000 \times g$  (Equitron) at 4 °C for 45 minutes. After ultracentrifugation, the supernatant was discarded and the pellet was resuspended in 1 mL of pH 6.8 phosphate buffer solution. 0.1 mL of this suspension was taken in a 5 mL volumetric flask, to which 0.5 mL isopropanol was added and the flask was shaken well. Subsequently, phosphate buffer was added to make up the volume of the solution to 5 mL.

## Results and discussion

### Structural characterization of niosomes

**DLS and TEM study.** For the structural characterization of the TW20:cholesterol (1:1) niosomes, we used dynamic light scattering (DLS) and transmission electron microscopy (TEM) imaging techniques. DLS studies enable the estimation of size ranges in nanometric dimensions in solution. Fig. 1 shows the size distribution histogram of the TW20:cholesterol (1:1) niosomes, as obtained from DLS measurements at 25 °C. The average size of the small unilamellar vesicles (niosome) was 118 nm with a narrow size distribution (100–150 nm), which is well correlated with the literature reported value (100–200 nm).<sup>17,18</sup> The temperature-dependent DLS histogram of the niosomes is represented in Fig. S6 (ESI†). It can be observed that with an increase in temperature there is a slight variation in the niosomal diameter from 124 to 161 nm. Fig. 2 shows the TEM images of the niosomes. The size of SUVs found from the microscopy images was  $\sim 125$  nm. The average niosome size obtained from the TEM image was almost equal to the size obtained from the DLS measurements. The clustering of niosomes, as seen in the image, appears to be a result of the drying process during sample preparation for TEM.

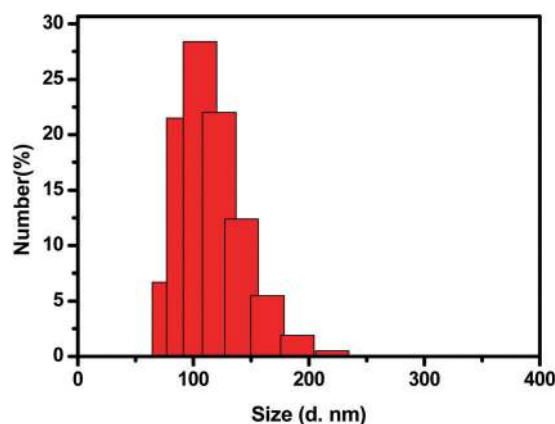


Fig. 1 DLS histogram plot for the TW20:cholesterol (1:1) niosomes at room temperature.

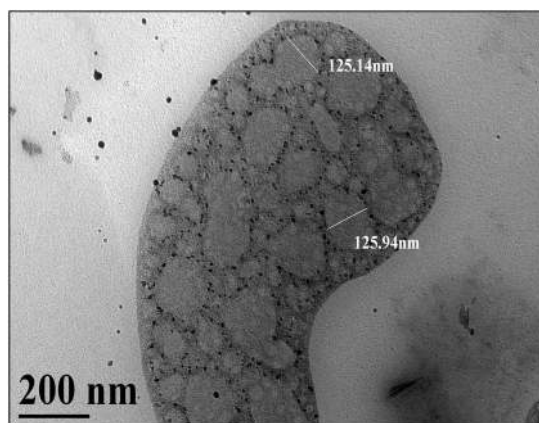


Fig. 2 A TEM image of the TW20:cholesterol (1:1) niosomes.

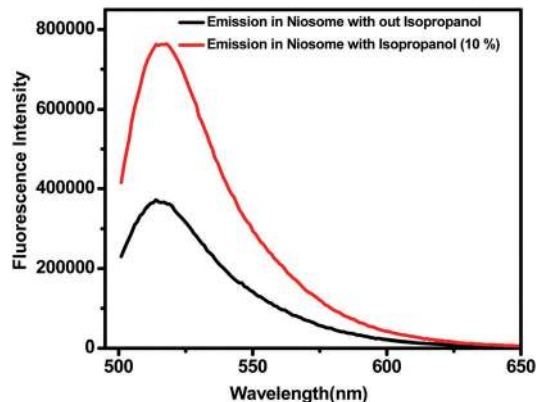


Fig. 3 Emission spectra of 5-carboxyfluorescein in niosomes with and without iso propanol (10%) (v/v). ( $\lambda_{\text{ex}} = 492 \text{ nm}$ ,  $\lambda_{\text{em}} = 515 \text{ nm}$ ) [5-carboxy-fluorescein] =  $1.41 \times 10^{-6} \text{ M}$ , slit width = 5 nm.

**Study on the aqueous compartment of niosomes.** In order to show the vesicular nature of the particles, 5-carboxyfluorescein (5-CF) release study was carried out. 5-CF is hydrophilic and strongly fluorescent in dilute aqueous solutions, but it shows significant concentration quenching of fluorescence.<sup>26</sup> The release of encapsulated 5-CF by isopropanol-induced membrane rupture, and the consequent dilution of 5-CF causes the fluorescence intensity to increase.<sup>27</sup> Fig. 3 shows the emission spectra of the same amount of 5-CF encapsulated niosomes in the presence and absence of isopropanol. The significant increase in the fluorescence intensity of 5-CF after the breaking of niosome vesicles gives evidence for the presence of an aqueous compartment within it.

**Calculation of entrapment efficiency.** The entrapment efficiency of the niosomal dispersion was calculated by separating the untrapped 5-CF using an ultracentrifugation method. The process of ultracentrifugation separates the niosomal dispersion into a supernatant part (upper liquid) and a pellet part (bottom solid). The supernatant part was used to record UV-visible absorption spectra. Here, instead of fluorescence intensity, the absorbance value was used for the calculation of entrapment efficiency because the pellet part was diluted several times in the fluorescence study to avoid the self-quenching nature of 5-CF. By considering the initial concentration of 5-CF loaded in the niosomes ( $10^{-5} \text{ M}$ ), the absorbance value of the supernatant (0.7567) and the molar extinction coefficient value of 5-CF (88 000), the encapsulation efficiency was calculated using the following equation.<sup>26</sup>

$$\begin{aligned} \text{Encapsulation efficiency} &= \frac{\text{Amount of fluorophore in niosomes}}{\text{Amount of fluorophore used}} \times 100 \\ &= \frac{\text{Concentration of fluorophore in niosomes}}{\text{Concentration of fluorophore used}} \times 100 \end{aligned} \quad (2)$$

The encapsulation efficiency of 5-CF in the niosomes was found to be 14.1% as calculated using the above equation.

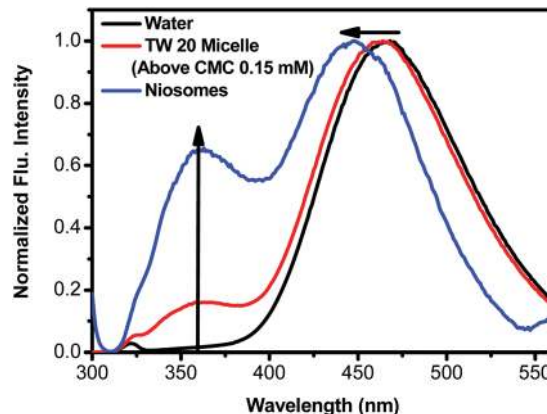


Fig. 4 A plot of the emission of 1-NpOH in water, TW20 micelles, and TW20:cholesterol (1:1) niosomes. [1-NpOH] =  $4 \mu\text{M}$ ,  $\lambda_{\text{ex}} = 290 \text{ nm}$ . Slit width = 5 nm.

### Fluorescence intensity study

#### Fluorescence intensity study of 1-NpOH in TW20 micelles.

In order to understand the fluorescence of 1-NpOH in the niosomes, a control set of experiments was carried out in TW20 micellar media. At lower concentrations of TW20, 1-NpOH possesses only anionic emission (470 nm) (Fig. S1A and B, ESI†). This spectral shape is consistent up to 0.05 mM of TW20, which is close to the reported critical micellar concentration (CMC).<sup>28</sup> Above CMC {above 0.05 mM [TW20]} the fluorescence intensity of NpOH\* (365 nm) increases, along with a small increase in the NpO<sup>-\*</sup> emission intensity (Fig. S1A, ESI†). The NpO<sup>-\*</sup> to NpOH\* intensity ratio decreases with an increase in the concentration of TW20 surfactants up to the CMC (0.05 mM), and after the CMC (above 0.05 mM) it almost remains constant (Fig. S1C, ESI†). The excited state deprotonation rate of 1-NpOH is significantly retarded above the CMC of the TW20 micelles, resulting in a substantial enhancement of NpOH\* intensity compared with its emission intensity in water (Fig. 4). The reduction in the ESPT rate is ascribed to the lower accessibility of the water molecule around 1-NpOH, engaged in the micelles as observed earlier in the micellar system.<sup>1,29</sup>

**Fluorescence study of 1-NpOH in TW20:cholesterol (1:1) niosomes.** A fluorescence study of 1-NpOH in several nano and micro-scale organized media has suggested that the fluorescence maximum at  $\sim 360 \text{ nm}$  is due to the neutral form (NpOH\*) emission, and the emission in the 450–460 nm range is due to the anionic form (NpO<sup>-\*</sup>) emission.<sup>23,30,31</sup> Like other organized media, 1-NpOH is also dual emissive in nature in niosomes. Such emissive behavior from the two prototypic forms is very similar to that observed in liposome media.<sup>23</sup> However, in contrast to the relatively lower fluorescence intensity ratio of the two prototypic forms ( $I_{\text{NpOH}^*}/I_{\text{NpO}^{*-}}$ ) in liposomic media, the ratio in niosomes is much higher. Incorporation of 1-NpOH into the niosome membrane leads to a significant enhancement of its NpOH\* intensity with a considerable blue shift in its NpO<sup>-\*</sup> intensity (445 nm) compared with the emission in water and TW20 micellar media. This suggests a substantial retardation of the ESPT process in highly nonpolar and confined microenvironments

of TW20: cholesterol (1:1) niosome membrane compared with TW20 micellar media.

**Temperature-dependent fluorescence intensity of 1-naphthol in niosomes.** Fig. 5 represents the temperature-dependent fluorescence spectral variation of 1-NpOH in TW20: cholesterol (1:1) niosomes. The figure shows a decrease in both  $\text{NpOH}^*$  and  $\text{NpO}^{*-}$  fluorescence with an increase in temperature, with the relative extent of the decrease being much higher for  $\text{NpOH}^*$  (Fig. 5A and Fig. S5, ESI†). Two possible explanations for rationalizing the drop in overall fluorescence intensity are: (i) expulsion of 1-NpOH from the niosome membrane domain to bulk water and (ii) a temperature-induced increase in the nonradiative decay rates of fluorescence. A clearer understanding of this requires a fluorescence lifetime study, which will be discussed later. However, the significant drop in the  $\text{NpOH}^*$  fluorescence indicates an increase in the deprotonation efficiency of  $\text{NpOH}^*$  with temperature. This appears to be similar to the observation in the liquid crystalline phase of liposome media,<sup>31</sup> where the increased availability of water at the membrane water interface was attributed to the increase in  $\text{NpO}^{*-}$  formation. The intensity ratio plot of the prototropic forms (Fig. 5B) increases with an increase in temperature and approaches saturation at higher temperatures. A clearer understanding of this aspect requires a close study of the fluorescence lifetime parameters, which will be discussed subsequently.

The second feature of Fig. 5 is the shift of the  $\text{NpO}^{*-}$  fluorescence maximum with temperature. The emission maximum of  $\text{NpO}^{*-}$  in water is  $\sim 470$  nm.<sup>12</sup> Being a charged species, it is known to show fluorescence solvatochromism and shifts to the blue region in a nonpolar medium.<sup>30</sup> Hence, the progressive shift of  $\text{NpO}^{*-}$  from 445 nm at 10 °C to 462 nm at 60 °C (Fig. S4, ESI†) indicates a progressive increase in the local polarity of the membrane domain with temperature. Thus, the twin observation of the (i) relative decrease in  $\text{NpOH}^*$  emission due to deprotonation and (ii) red shift of  $\text{NpO}^{*-}$  emission point out an increase in the availability of water in the membrane domain at higher temperatures.

The third observation, which is noteworthy, is that the temperature-induced changes of the ESPT behavior of NpOH were fairly regular in the temperature interval studied (Fig. 5A).

The absence of a significant change in the spectral feature in a narrow temperature range ( $\leq 2$  °C) strongly implies the absence of thermotropic phase change behavior in this niosome.

Some niosomes formed with nonionic surfactant and cholesterol (1:1) mixtures are known to show thermotropic phase transition behavior between the ordered gel phase at lower temperatures and the less order liquid crystal phase at higher temperatures; the phase transition occurs in the range of 30–45 °C for different systems.<sup>16,32–34</sup> There are also reports of surfactant:cholesterol niosomes not showing thermotropic phase change behavior.<sup>17,21,22</sup> The niosomes in this study, TW20: cholesterol (1:1), seem to belong to the latter category. A possible reason for the lack of phase transition behavior may lie in the structure of the TW20 molecule, which has a fairly large polar head group and a relatively short alkyl tail. The requirement of adequate hydrophobicity for the formation of a bilayer system is fulfilled by cholesterol, which is known to smother the thermotropic phase transition in liposomes.<sup>31</sup>

**Fluorescence lifetime study.** Fluorescence lifetime decays of  $\text{NpOH}^*$  and  $\text{NpO}^{*-}$  show bi-exponential fitting with shorter ( $\tau_s$ ) and longer lifetime ( $\tau_l$ ) components (Fig. S2 and S3, ESI†) in the TW20: cholesterol (1:1) niosome membrane. For similar observations, Sujatha *et al.* proposed a two-state model to explain the fluorescence lifetime and population distribution of both forms of 1-NpOH in liposomes.<sup>32</sup> According to that model, the  $\tau_l$  of  $\text{NpOH}^*$  ( $\tau_l^{\text{neutral}}$ ) originates from the nonpolar membrane core region and the  $\tau_s$  of  $\text{NpOH}^*$  ( $\tau_s^{\text{neutral}}$ ) originates from the semi-polar and water accessible membrane interface region. For  $\text{NpO}^{*-}$ , the  $\tau_l$  ( $\tau_l^{\text{anion}}$ ) originates from the membrane interface region and the  $\tau_s$  ( $\tau_s^{\text{anion}}$ ) originates from the unpartitioned 1-NpOH present in the aqueous medium.<sup>23,31</sup> As niosomes have almost the same structural and physical properties as liposomes, it is expected that 1-NpOH is distributed in niosomes in a similar manner and shows similar fluorescence lifetime behavior to liposomes.

Schemes 3 and 4 represent the distributive nature of 1-NpOH in different regions of the niosome membrane (the dry core region, interface region, and bulk water region). It is observed that naphthol molecules present in the bulk water emit only anionic emission, and from the core region they emit

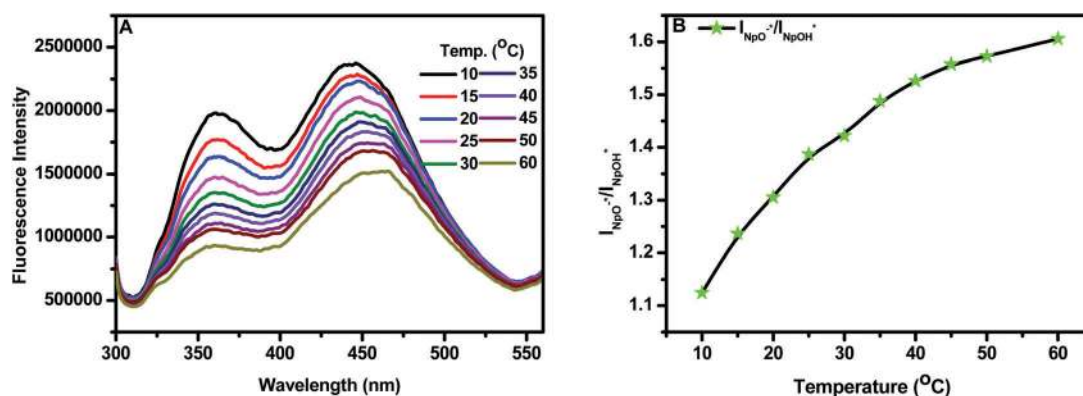
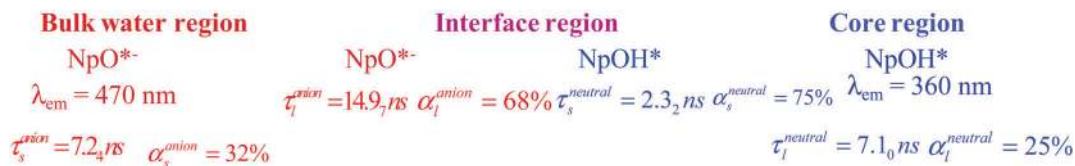


Fig. 5 (A) Emission spectra of 1-NpOH in the niosome membrane with varying temperature and (B) plot of the fluorescence intensity ratio ( $I_{\text{NpO}^{*-}}/I_{\text{NpOH}^*}$ ) of 1-NpOH in the niosome membrane with the variation of temperature. [1-NpOH] = 4  $\mu\text{M}$ ,  $\lambda_{\text{ex}}$  = 290 nm (error =  $\pm 3\%$ ). Slit width = 5 nm.

## Different regions in Niosome membrane



Scheme 3 Fluorescence lifetime values for both the anionic and neutral species distributed in the different regions of the niosome membrane at 30 °C.  $\lambda_{\text{ex}} = 290 \text{ nm}$ .

only neutral emission, whereas the interfacial location of 1-NpOH results in both anionic and neutral emissions. Because of the distributive nature of 1-NpOH, the anionic and neutral emission follow biexponential fitting in niosomes. The anionic species are distributed in the bulk water region and interface whereas the neutral species are distributed in the interface and niosomal core (Scheme 3). The amplitude of both the prototropic emissions originating from the interfacial region is larger than the corresponding amplitude that originates from the bulk water (for anionic species) and niosomal core region (for neutral species). From this observation, it can be concluded that the preferential location of 1-NpOH in the niosome membrane is at the interface, as compared to bulk water and the core.

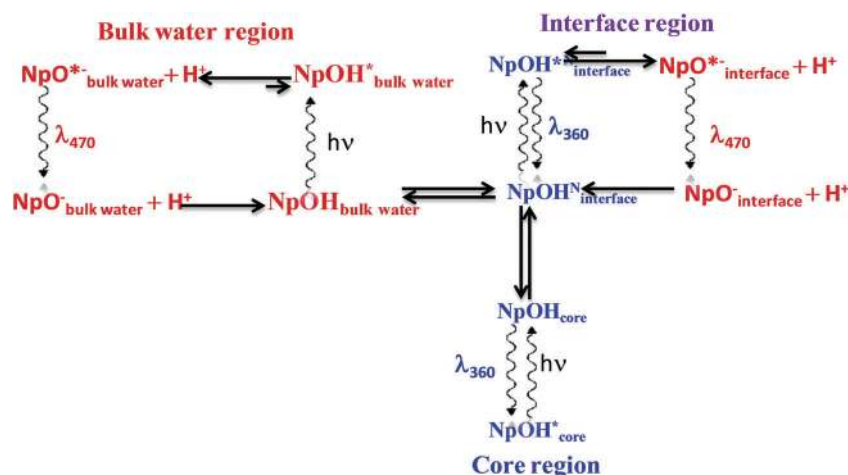
**Temperature-dependent fluorescence lifetime study of 1-NpOH in niosomes.** The following observations can be made from scrutiny of the data.

(i) For anionic emission of 1-naphthol ( $\text{NpO}^{*-}$ ), the lifetime value of the shorter component almost remains constant, whereas the lifetime value of the longer component decreases with temperature. On the other hand, the relative amplitude of the shorter component increases with a concomitant decrease for the longer component (Table 1).

(ii) For the neutral emission of  $\text{NpOH}^*$ , the lifetime value of the shorter component decreases, whereas the lifetime value of the longer component almost remains constant. The relative amplitude of both components remains constant throughout the temperature range (20–60 °C) (Table 2).

Fluorescence lifetime data of  $\text{NpO}^{*-}$  in Table 1 show that the longer lifetime component ( $\tau_1^{\text{anion}}$ ) decreases from 15.9<sub>9</sub> ns (20 °C) to 11.9<sub>5</sub> ns (60 °C) and the shorter lifetime component ( $\tau_s^{\text{anion}}$ ) almost remains constant ( $\sim 7 \text{ ns}$ ) with temperature. This significant decrease in the  $\tau_1^{\text{anion}}$  lifetime indicates that there is an increase in nonradiative decay processes upon going from a lower to a higher temperature. This may be the possible reason for the decrease in  $\text{NpO}^{*-}$  fluorescence with temperature. In water and TW20 micellar medium,  $\text{NpO}^{*-}$  shows a mono-exponential fit with a fluorescence lifetime of 7.6<sub>8</sub> ns (Table S1, ESI<sup>†</sup>), thus  $\tau_s^{\text{anion}}$  is ascribed to the unpartitioned 1-NpOH present in the aqueous phase. The  $\sim 16 \text{ ns}$  ( $\tau_1^{\text{anion}}$ ) component, which is very similar to the  $\sim 18 \text{ ns}$  component of anion emission originating from the liposome interface,<sup>24</sup> can be assigned to the  $\text{NpO}^{*-}$  originating from the water accessible interfacial region of the niosome membrane. The relative amplitude of  $\tau_1^{\text{anion}}$  decreases with an increase in the relative amplitude of  $\tau_s^{\text{anion}}$  of  $\text{NpO}^{*-}$  (Table 1) with an increase in temperature. This confirms the expulsion of 1-NpOH from the membrane interfacial region to bulk water. The fluorescence lifetime data of  $\text{NpOH}^*$  in Table 2 show that the lifetime of the shorter component ( $\tau_s^{\text{neutral}}$ ) decreases from 2.6<sub>6</sub> ns to 1.7<sub>3</sub> ns and the lifetime of the longer component ( $\tau_1^{\text{neutral}}$ ) ( $\sim 7 \text{ ns}$ ) almost remains constant with temperature. The relative amplitudes of  $\tau_s^{\text{neutral}}$  and  $\tau_1^{\text{neutral}}$  almost remain constant with temperature (Table 2).

Monalisa *et al.* showed that the fluorescence lifetime of 1-NpOH efficiently sensed the hydration of the lipid bilayer



Scheme 4 Scheme of the prototropism and consequent fluorescence of 1-naphthol (ROH) in a niosome suspension.

**Table 1** Fluorescence lifetime data of  $\text{NpO}^{*-}$  with an increase in the temperature of the TW20 : cholesterol (1 : 1) niosomes ( $\lambda_{\text{ex}} = 295 \text{ nm}$ ,  $\lambda_{\text{em}} = 460 \text{ nm}$ ). [1-NpOH] = 4  $\mu\text{M}$ . (Error =  $\pm 5\%$ ). Here,  $\tau_1 = \tau_s^{\text{anion}}$ ,  $\alpha_1 = \alpha_s^{\text{anion}}$ ,  $\tau_2 = \tau_l^{\text{anion}}$ ,  $\alpha_2 = \alpha_l^{\text{anion}}$

$E_m = 460 \text{ nm}$ Temp. ( $^{\circ}\text{C}$ )	$\tau_1(\alpha_1)$	$\tau_2(\alpha_2)$	$\tau_{\text{avg}}$	$\chi^2$
20	7.2 <sub>7</sub> (25)	15.9 <sub>9</sub> (75)	14.8 <sub>4</sub>	1.32
30	7.2 <sub>4</sub> (32)	14.9 <sub>7</sub> (68)	13.5 <sub>3</sub>	1.27
40	7.1 <sub>9</sub> (41)	13.9 <sub>8</sub> (59)	12.1 <sub>9</sub>	1.39
50	6.9 <sub>7</sub> (45)	12.8 <sub>6</sub> (55)	11.0 <sub>5</sub>	1.26
60	6.6 <sub>9</sub> (52)	11.9 <sub>5</sub> (48)	9.9 <sub>6</sub>	1.25

**Table 2** Fluorescence lifetime data for  $\text{NpOH}^*$  with an increase in the temperature of the TW20 : cholesterol (1 : 1) niosomes ( $\lambda_{\text{ex}} = 295 \text{ nm}$ ,  $\lambda_{\text{em}} = 360 \text{ nm}$ ), [1-NpOH] = 4  $\mu\text{M}$ . (Error =  $\pm 5\%$ ). Here,  $\tau_1 = \tau_s^{\text{neutral}}$ ,  $\alpha_1 = \alpha_s^{\text{neutral}}$ ,  $\tau_2 = \tau_l^{\text{neutral}}$ ,  $\alpha_2 = \alpha_l^{\text{neutral}}$

$E_m = 360 \text{ nm}$ Temp. ( $^{\circ}\text{C}$ )	$\tau_1(\alpha_1)$	$\tau_2(\alpha_2)$	$\tau_{\text{avg}}$	$\chi^2$
20	2.6 <sub>6</sub> (74)	6.9 <sub>6</sub> (26)	4.7 <sub>1</sub>	1.43
30	2.3 <sub>2</sub> (75)	7.1 <sub>0</sub> (25)	4.7 <sub>3</sub>	1.23
40	2.0 <sub>5</sub> (75)	7.1 <sub>8</sub> (25)	4.8 <sub>1</sub>	1.20
50	1.8 <sub>8</sub> (74)	7.0 <sub>1</sub> (26)	4.7 <sub>8</sub>	1.30
60	1.7 <sub>3</sub> (72)	7.0 <sub>3</sub> (28)	4.9 <sub>7</sub>	1.25

membrane with an increase in the bile salt concentration.<sup>23</sup> According to that study, the increase in hydration at the interfacial region of the membrane leads to a decrease in  $\tau_s^{\text{neutral}}$  and  $\tau_l^{\text{anion}}$  (both originating from the interfacial sites of the membrane), with no change in the  $\tau_l^{\text{neutral}}$  (which originates from the core sites of the membrane).<sup>23</sup> In our study, we have observed that there is a decrease in the  $\tau_s^{\text{neutral}}$  (Table 2) as well as the  $\tau_l^{\text{anion}}$  with temperature. Hence, this observation suggests that hydration at the interfacial region of niosomes increases with increasing temperature. The constant  $\tau_l^{\text{neutral}}$  (Table 2) suggests that the hydrophobic core region of niosomes seems to be unaffected and remains dry with temperature. In this regard, these niosomes behaves differently to liposomes, which can form by association of a single amphiphilic molecular species

like a lipid.<sup>14</sup> The association of cholesterol with the hydrocarbon moiety of TW20 forms the core part of this niosome membrane. The greater thickness of the membrane compared with liposomes may also have a role to play in this behavior.<sup>19</sup>

**Lifetime distribution analysis.** Fluorescence lifetime distribution analysis provides valuable information on the heterogeneity of the environment around a particular fluorescing species, with a broader distribution implying greater heterogeneity.

Fig. 6 shows the fluorescence lifetime distribution plot for  $\text{NpO}^{*-}$  with variation of temperature in TW20 : cholesterol (1 : 1) niosomes. The ‘full width at half maximum’ (FWHM) value of both the shorter and longer components decreases with temperature (Table 3). There is a significant drop in the modal time (15.9<sub>5</sub>–10.6<sub>7</sub>) of the longer component, whereas this drop is not very significant for the shorter component (8.5<sub>3</sub>–6.8<sub>5</sub>) (Table 3). The distribution plot of the longer component (originated from the interfacial region) becomes narrower with an increase in temperature, indicating that at lower temperatures, the local environmental heterogeneity sensed by 1-NPOH at the interfacial region of the niosome membrane is greater and it becomes more homogeneous with increasing temperature (Fig. 6A). The distribution plot of the shorter component also has a similar trend, although it is less significant.

Fig. 7 shows the fluorescence lifetime distribution plot for  $\text{NpOH}^*$  with an increase of temperature in the TW20 : cholesterol (1 : 1) niosome membrane. The variation in the FWHM value for the longer component was negligible, whereas it was considerable for the shorter lifetime component (Table 4). The modal time of the shorter component decreased, whereas for the longer component this value almost remained constant ( $\sim 7 \text{ ns}$ ) (Table 4), which agrees with the fluorescence lifetime values obtained using iterative reconvolution (Table 2). The distribution plot is narrow for the longer component, whereas for the shorter component it is broader. These distribution profiles give information about the heterogeneity in the surrounding environment sensed by 1-naphthol in niosomes: the narrow distribution of the longer component (originating from the core region) indicates that the environment sensed by 1-naphthol in

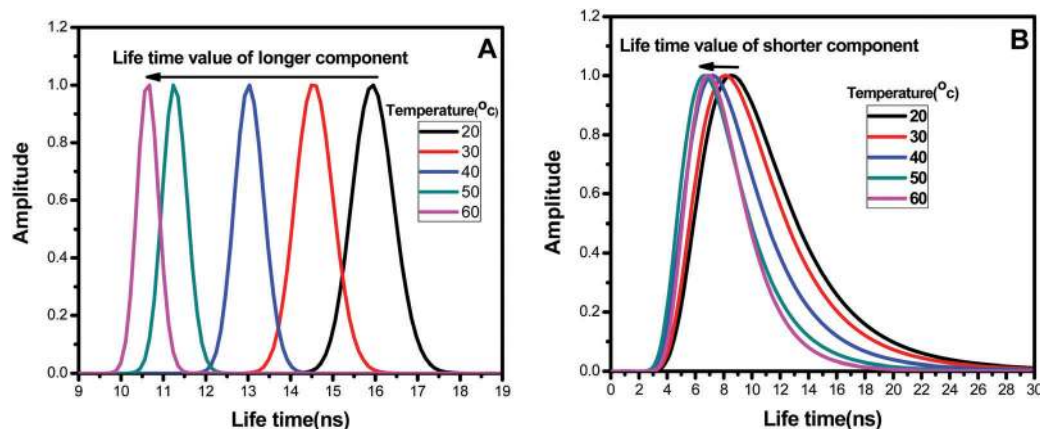


**Fig. 6** A fluorescence lifetime distribution plot of (A) the longer component ( $\tau_l^{\text{anion}}$ ) and (B) the shorter component ( $\tau_s^{\text{anion}}$ ) for  $\text{NpO}^{*-}$  with variation of temperature in TW20 : cholesterol (1 : 1) niosomes. [1-NpOH] = 4  $\mu\text{M}$ ,  $\lambda_{\text{ex}} = 295 \text{ nm}$ ,  $\lambda_{\text{em}} = 460 \text{ nm}$ .

**Table 3** Fluorescence lifetime distribution data for NpO<sup>−</sup>\* with an increase in the temperature of the TW20 : cholesterol (1 : 1) niosomes. [1-NpOH] = 4 μM. λ<sub>ex</sub> = 295 nm, λ<sub>em</sub> = 460 nm, (error = ±5%). (FWHM<sub>S</sub> = full width at half maximum of the shorter component, FWHM<sub>L</sub> = Full width at half maximum of the longer component)

Temperature (°C)	FWHM <sub>S</sub>	FWHM <sub>L</sub>	Modal time <sub>S</sub>	Modal time <sub>L</sub>	χ <sup>2</sup>
20	7.34	1.15	8.5 <sub>3</sub>	15.9 <sub>5</sub>	1.39
30	6.90	1.06	8.0 <sub>8</sub>	14.4 <sub>6</sub>	1.25
40	6.10	0.82	7.1 <sub>8</sub>	13.0 <sub>3</sub>	1.27
50	5.25	0.69	6.6 <sub>2</sub>	11.2 <sub>3</sub>	1.28
60	4.74	0.60	6.8 <sub>5</sub>	10.6 <sub>7</sub>	1.28

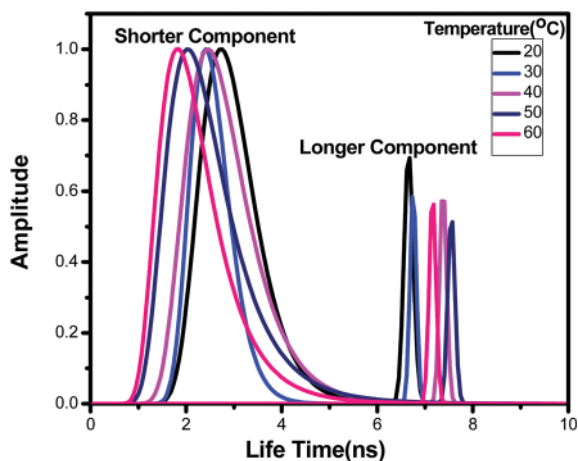


**Fig. 7** Fluorescence lifetime distribution plot for NpOH\* (360 nm) with variation of temperature in TW20 : cholesterol (1 : 1) niosomes. [1-NpOH] = 4 μM, λ<sub>ex</sub> = 295 nm, λ<sub>em</sub> = 360 nm.

**Table 4** Fluorescence lifetime distribution data for NpOH\* with an increase in the temperature of the TW20 : cholesterol (1 : 1) niosomes [1-NpOH] = 4 μM, λ<sub>ex</sub> = 295 nm, λ<sub>em</sub> = 360 nm, (error = ±5%)

Temperature (°C)	FWHM <sub>S</sub>	FWHM <sub>L</sub>	Modal time <sub>S</sub>	Modal time <sub>L</sub>	χ <sup>2</sup>
20	1.34	0.23	2.7 <sub>4</sub>	6.6 <sub>7</sub>	1.27
30	1.05	0.16	2.4 <sub>1</sub>	6.7 <sub>3</sub>	1.20
40	1.50	0.18	2.4 <sub>6</sub>	7.3 <sub>4</sub>	1.11
50	1.43	0.18	2.0 <sub>1</sub>	7.5 <sub>7</sub>	1.30
60	1.35	0.17	1.7 <sub>9</sub>	7.1 <sub>8</sub>	1.36

the niosomal core region remains unchanged throughout the temperature range (20–60 °C). On the other hand, the wider distribution plot of the shorter component (originating from the interfacial region) indicates that at the interfacial region there is heterogeneity in the surrounding environment sensed by 1-NpOH.

The rates of proton transfer of NpOH\* with variation of temperature in the niosome membrane were calculated using eqn (3),<sup>35</sup>

$$k_{pt} = \frac{1}{\tau} - \frac{1}{\tau_0} \quad (3)$$

where  $k_{pt}$  represents the ESPT rate constant and  $\tau_0$  is the lifetime value of 1-NpOH in the absence of the ESPT process. The longer lifetime component of NpOH\* originating from

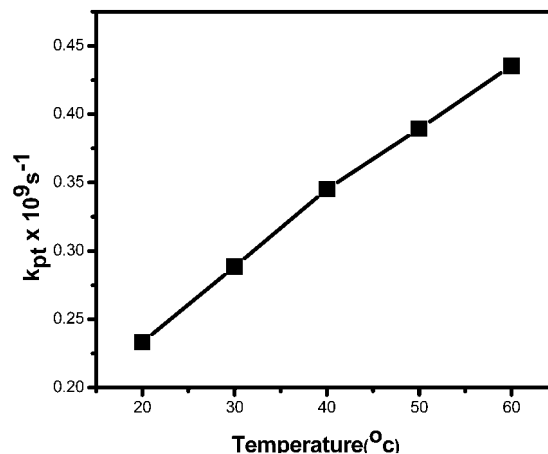


**Fig. 8** A plot of variation in the ESPT rate constant ( $k_{pt}$ ) of NpOH\* with variation of temperature (for the shorter lifetime component) in the niosome membrane. [1-NpOH] = 4 μM.

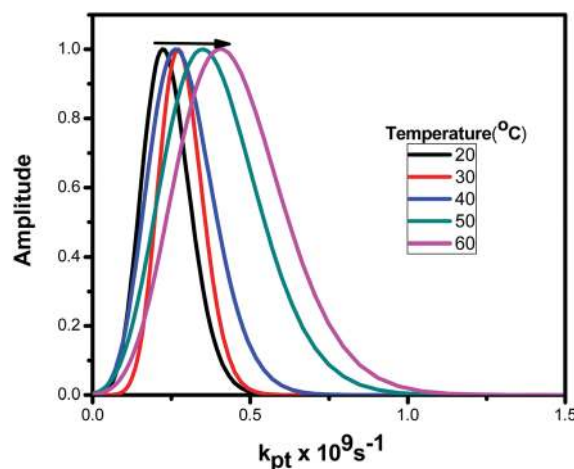


**Fig. 9** A plot of the proton transfer rate ( $k_{pt}$ ) with amplitude of NpOH\* with variation of temperature (for the shorter lifetime component obtained from the distribution plot) in the niosome membrane. [1-NpOH] = 4 μM.

the membrane core region is considered as  $\tau_0$  for the calculation of  $k_{pt}$  with variation of temperature. The value of  $k_{pt}$  increases with an increase in temperature (Fig. 8). The rate of proton transfer of 1-NpOH is strongly dependent on the availability of water molecules around it.<sup>21</sup> The increased value of  $k_{pt}$  with variation in temperature successfully reflects the penetration of water into the interfacial region of the niosome membrane.

Fig. 9 represents the plot of  $k_{pt}$  vs. the fluorescence lifetime amplitude (which corresponds to a shorter lifetime component of NpOH\* as obtained from nonextensive lifetime distribution fitting) with variation of temperature. Here, the interesting observation is that with an increase in the temperature, there is a broadening in the spectral shape in the distribution plot. This broadening indicates that the rate of proton transfer increases with an increase in temperature, which follows the same trend as the proton transfer rate given in Fig. 8.

## Conclusions

In this work, the high sensitivity of 1-NpOH fluorescence to the presence of water in its microenvironment has been successfully used to monitor the temperature-dependent changes in the niosomal membrane (TW20: cholesterol (1:1)). The changes in fluorescence lifetimes and amplitudes for the two prototropic forms (NpOH\*, NpO<sup>-</sup>\*) and their distribution plots indicate significant wetting of the interfacial region by keeping the core region of the niosome unaffected. The increase in the proton transfer rate of NpOH\* with temperature provides additional evidence about the interfacial wetting of the niosome membrane. With increasing temperature, 1-NpOH appears to get expelled from the niosome to the bulk water medium. The other interesting observation is the absence of any phase transition behavior of this niosome system.

## Acknowledgements

This research was supported by a research project funded by the Department of Science and Technology, Government of India. The authors thank Dr E. Prasad, Department of Chemistry, IIT Madras, for his kind help in carrying out the DLS experiments. The authors also thank SAIF IITM and the Metallurgical and Materials Engineering Department IITM for the TEM images. J.S. thanks DST for his fellowship. J.M. thanks IIT Madras for her research fellowship.

## References

- 1 A. K. Mishra, in "Understanding and Manipulating Excited State Processes", *Molecular and Supramolecular Photochemistry Series*, ed. V. Ramamurthy and K. S. Schanze, Marcel Dekker, Inc., New York, 2001, ch. 10, 8, p. 577.
- 2 P. Dutta and K. Bhattacharyya, *J. Chem. Sci.*, 2004, **116**, 5–16.
- 3 E. Pines, *UV-Visible Spectra and Photoacidity of Phenols, Naphthols and Pyrenols*, John Wiley & Sons, 2009.
- 4 S. P. Webb, L. A. Philips, S. W. Yeh, L. M. Tolbert and J. H. Clark, *J. Phys. Chem.*, 1986, **90**, 5154–5164.
- 5 J. Lee, R. D. Griffin and G. W. Robinson, *J. Chem. Phys.*, 1985, **82**, 4920–4925.
- 6 G. W. Robinson, P. J. Thistlethwaite and J. Lee, *J. Phys. Chem.*, 1986, **90**, 4224–4233.
- 7 A. C. Kumar and A. K. Mishra, *Talanta*, 2007, **71**, 2003–2006.
- 8 D. Sukul, S. K. Pal, D. Mandal, S. Sen and K. Bhattacharyya, *J. Phys. Chem. B*, 2000, **104**, 6128–6132.
- 9 P. Dutta, A. Halder, S. Mukherjee, P. Sen, S. Sen and K. Bhattacharyya, *Langmuir*, 2002, **18**, 7867–7871.
- 10 R. A. Agbaria, B. Uzank and P. Gill, *J. Phys. Chem.*, 1989, **93**, 3855–3859.
- 11 J. Sujatha and A. K. Mishra, *J. Photochem. Photobiol., A*, 1996, **101**, 215–219.
- 12 J. Lee, G. W. Robinson, S. P. Webb, L. A. Philips and J. H. Clark, *J. Am. Chem. Soc.*, 1986, **108**, 6538–6542.
- 13 N. Pappayee and A. K. Mishra, *Spectrochim. Acta, Part A*, 2000, **56**, 2249–2253.
- 14 M. Mohapatra and A. K. Mishra, *J. Phys. Chem. B*, 2010, **114**, 14934–14940.
- 15 T. Varun, A. Sonia, P. Bharat and V. Patil, *Int. J. Pharm. Chem. Sci.*, 2012, **1**, 981–993.
- 16 I. F. Uchebgu and S. P. Vyas, *Int. J. Pharm.*, 1998, **172**, 33–70.
- 17 S. Mandal, C. Banerjee, S. Ghosh, J. Kuchlyan and N. Sarkar, *J. Phys. Chem. B*, 2013, **117**, 6957–6968.
- 18 G. P. Kumar and P. Rajeshwarrao, *Acta Pharm. Sin. B*, 2011, **1**, 208–219.
- 19 M. J. Lawrence, in *Sorbitan esters (sorbitan fatty acid esters)*, ed. R. C. Rowe, P. L. Sheskey and P. L. Weller, Handbook of pharmaceutical excipients, Pharmaceutical Press, London, UK, 4th edn, 2003.
- 20 T. Liu and R. Guo, *Langmuir*, 2005, **21**, 11034–11039.
- 21 T. Mondal, S. Ghosh, A. K. Das, A. K. Mandal and K. Bhattacharyya, *J. Phys. Chem. B*, 2012, **116**, 8105–8112.
- 22 S. Mandal, V. G. Rao, C. Ghatak, R. Pramanik, S. Sarkar and N. Sarkar, *J. Phys. Chem. B*, 2011, **115**, 12108–12119.
- 23 M. Mohapatra and A. K. Mishra, *J. Phys. Chem. B*, 2010, **114**, 14934–14940.
- 24 D. Pozzi, R. Caminiti, C. Marianecchi, M. Carafa, E. Santucci, S. C. De Sanctis and G. Caracciolo, *Langmuir*, 2010, **26**, 2268–2273.
- 25 I. F. Uchebgu and A. T. Florence, *Adv. Colloid Interface Sci.*, 1995, **58**, 1–55.
- 26 R. F. Chen and J. R. Knutson, *Anal. Biochem.*, 1988, **172**, 61–77.
- 27 I. F. Uchebgu, A. Schätzlein, G. Vanlerberghe, N. Morgatini and A. T. Florence, *J. Pharm. Pharmacol.*, 1997, **49**, 606–610.
- 28 M. Essa Mahmood and D. A. F. Al-Koofee, *Global Journal of Science Frontier Research Chemistry*, 2013, **13**, 1–7.
- 29 D. Mandal, S. K. Pal and K. Bhattacharyya, *J. Phys. Chem. A*, 1998, **102**, 9710–9714.
- 30 J. Swain and A. K. Mishra, *Phys. Chem. Chem. Phys.*, 2015, **17**, 16752–16759.
- 31 J. Sujatha and A. K. Mishra, *Langmuir*, 1998, **14**, 2256–2262.
- 32 C. S. Chaw and K. Y. Ah Kim, *Pharm. Dev. Technol.*, 2013, **18**, 667–672.
- 33 W. Hua and T. Liu, *Colloids Surf., A*, 2007, **302**, 377–382.
- 34 H. Abdelkader, A. Kamal, S. Ismail and R. G. Alany, *Pharmazie*, 2010, **65**, 1–7.
- 35 Y. V. Il'ichev, K. M. Solntsev, M. G. Kuzmin and H. J. Lemmetyinen, *J. Chem. Soc., Faraday Trans.*, 1994, **90**, 2717–2724.
- 36 *Food Emulsifiers and Their Applications*, ed. G. L. Hasenhuettl and R. W. Hartel, 2008.